Int. J. Electrochem. Sci., 8 **(2013)** 8115 - 8125

International Journal of
ELECTROCHEMICAL
SCIENCE
www.electrochemsci.org

Calcium Phosphate/Titania Sol-Gel Coatings on AZ31 Magnesium Alloy for Biomedical Applications

Hui Tang[1], *Tiezhu Xin*[2,*], *Fuping Wang*[1,*]

[1] School of Chemical Engineering and Technology, Harbin Institute of Technology, Heilongjiang 150001, PR China
[2] School of Material Science and Engineering, Harbin Institute of Technology, Heilongjiang 150001, PR China
[*]E-mail: tiezhu-x@163.com; hitth001@yahoo.cn

Received: 7 March 2013 / *Accepted:* 18 May 2013 / *Published:* 1 June 2013

Calcium phosphate layer was coated onto AZ31 magnesium substrate with an insertion of a titania buffer layer by sol-gel method. The calcium phosphate layer was employed to enhance the bioactivity of the magnesium alloy, and the titania buffer layer was inserted to improve the bonding strength between the calcium phosphate layer and magnesium substrate, as well as to prevent the corrosion of the magnesium substrate. The structure and composition of the sol-gel coatings were characterized by scanning electron microscopy (SEM) and X-ray diffraction (XRD). The bonding strength, corrosion behaviors and the hydrogen evolution rate of the samples were also studied. The results showed that the sol-gel coatings improved the corrosion resistance and reduced the hydrogen evolution rate of the magnesium alloy in simulated body fluid (SBF) solution. The titania buffer layer could significantly improve the bonding strength and the corrosion resistance.

Keywords: Magnesium alloy; Calcium phosphate; Titania; Corrosion resistance; Hydrogen evolutio

1. INTRODUCTION

Recently, magnesium and its alloys have attracted great interest for biomedical applications, particularly as a biodegradable material for orthopedic implants [1-4]. Compared with the commonly used metallic biomaterials such as stainless steels and titanium alloys, magnesium alloys have many outstanding advantages. Firstly, the density, elastic modulus and yield strength of magnesium alloys are closer to that of the nature bone than the other metallic materials, which could significantly reduce the "stress shielding" existed in the metallic bone implants [5]. Secondly, due to their biodegradability and bioabsorbability, the second surgery for removal of the metal bone plates and screws is not

necessary by using magnesium implants [6,7]. Furthermore, as an important element for human metabolism, magnesium is found in bone tissue [6]. Some studies have also demonstrated that the dissolved magnesium ions can promote bone cell attachment and tissue growth on the implants [8,9]. Many researchers have reported the in vitro and in vivo biocompatibility and biodegradability of magnesium based alloys [10,11]. However, the clinical application of Mg based implants at present are limited due to their relatively high degradation rate accompanied by hydrogen evolution under physiological conditions and limited bioactivity.

The main mineral component of bone is calcium deficient carbonate hydroxyapatite. Calcium phosphate coatings show the advantage in improving the biocompatibility of metallic implants and increasing bone growth at the site of implantation [12,13]. Therefore, many surface treatment techniques, including biomimetic method [14,15], hydrothermal treatment [16], chemical conversion [17], electrodeposition and sol-gel method [18-20] have been adopted to prepare calcium phosphate coating on magnesium alloys aiming at slowing down the biodegradation rate and improving the bioactivity. Among these technologies, the sol-gel method has been receiving more and more attention as it is an inexpensive, convenient and environmentally friendly technique. It can control the chemical composition, microstructure of the coatings and prepare homogeneous coatings [21]. But it is difficult for calcium phosphate coating to form chemical bond with magnesium substrate at the interface, because of their different lattice structure. Thus, many attempts have been made to produce a buffer layer to enhance the bonding strength between the calcium phosphate coating and the metallic substrate. Titanium oxide has been extensively investigated as biomaterial due to its excellent biocompatibility and superior corrosion resistance. Previous research showed that titania coatings between the calcium phosphate coating and titanium substrate could improve the bonding strength as well as the corrosion resistance of titanium [22]. The corrosion resistance increased while increasing the thickness of titania coating [21,23]. Therefore, calcium phosphate/titania coating can be expected to combine the advantages of the titania with those of calcium phosphate. The calcium phosphate layer is expected to enhance the bioactivity and osteoconductivity during the initial stage following implanatation, by acting as an outer coating layer. The inner titania layer is designed to prevent the Mg substrate from becoming corroded, even after the calcium phosphate layer has been completely dissolved due to biological process. More importantly, the titania layer acted as a buffer layer between the calcium phosphate layer and the Mg substrate , is expected to improve the bonding strength of the calcium phosphate layer with respect to the Mg substrate. Since the bonding strength of calcium phosphate coatings on Mg has been reported to be relatively low, improving the adhesive properties of the calcium phosphate coating on Mg substrate is essential for it used as implants. However, there is few literature about the study of calcium phosphate/titania coatings deposited on magnesium alloys.

In this present work, calcium phosphate/titania was coated onto AZ31 magnesium by sol-gel method, in order to control the degradation rate and at the same time to improve the bonding strength between the calcium phosphate coating and magnesium substrate. The electrochemical behavior and the degradation rate of the samples, as well as the bonding strength between the coating and the substrate were studied.

2. EXPERIMENTAL

2.1 Preparation of the coatings

AZ31 magnesium alloy specimens of size 20 mm × 20 mm × 5 mm were used in this investigation. The specimens were polished to 1200 grit emery finish, degreased in acetone, rinsed by ethanol and dried in cold air.

For the preparation of the titania sol, tetrabutylorthotitanate ($Ti(OCH_2CH_2CH_3)_4$) was diluted with absolute ethanol, and then a small amount of distilled water mixed with diethanolamine ($NH(CH_2CH_2OH)_2$) was added into the solution, followed by vigorous stirring for 24 h. Subsequently, the mixed sol was aged for 24 h. To make calcium phosphate sol, triethyl phosphate($(C_2H_5O)_3P$) and calcium nitrate ($Ca(NO_3)_2 \cdot 4H_2O$)) were selected as P and Ca sources, respectively. Triethyl phosphite diluted with anhydrous ethanol was hydrolysed with distilled water. Calcium nitrate dissolved in anhydrous ethanol was added to the hydrolysed phosphite sol which had been aged for 24 h (molar ratio Ca:P = 1.67). Vigorous stirring was continued for 4 h after the titration, and the mixed sol was aged for 12 h.

The AZ31 magnesium alloy substrate was dipped into tatania sol, a controlled linear positioner was used as a puller with the speed of 3 cm/min. The films were aged for 30 min at 60 ^oC before they were heated to 400 ^oC for 30 min. The process was repeated two times. And it was named as T coating. To prepare calcium phosphate/titania coating, the T coating was dipped into calcium phosphate sol, and pulled of at the speed of 3 cm/min. The samples were aged for 30 min at 60 ^oC before they were heated to 400 ^oC for 30min. The process was repeated two times, and it was named as HT coating. For comparison, the substrate dipped into calcium phosphate sol repeated the above process four times, and it was named as H coating.

2.2 Characterization of the coatings

Coating morphology and cross-section were observed using a Scanning electron microscope (SEM, S-4800, Hitachi Co., Japan). The element distribution on the surface of the coating was investigated by energy dispersive spectroscopy (EDS, Oxford Model 7537, England). XRD patterns of the coatings were studied by glancing incidence X-ray diffraction (GIXRD) (Philips, X'Pert, the Netherlands) using Cu Kα radiation. The angle of the incident was 2° against the surface of the sample with a continuous scanning mode at a rate of 4°/min.

2.3 The bonding strength

The adhesive strength of the coatings was determined by a pull-off method utilizing an Instron instrument. The average bonding strength value of five samples treated under the same condition was given as the means. The coated and the back side of the samples were attached to cylinders with epoxy resin. Tensile load was applied at a speed of 2 mm/min until fracture occurred. The pull-of force F and the contact area S was measured. The coating adhesion strength was estimated as F/S.

2.4 Electrochemical behaviors

Electrochemical measurements were performed in simulated body fluid (SBF) at a temperature 37 ^{o}C. A three-electrode cell with the samples as the working electrodes was used for the electrochemical testing. A platinum electrode was used as counter electrode, and a saturated calomel electrode served as reference electrode. The SBF solution was prepared by dissolving analytical-grade chemicals of NaCl, KCl, Na_2SO_4, $NaHCO_3$, $K_2HPO_4 \cdot 3H_2O$, $MgCl_2 \cdot 6H_2O$ and $CaCl_2$ in distilled water and buffered at pH 7.4 with tris-hydroxymethyl aminomethan and 1 M HCl at 37 ^{o}C, with ionic concentrations (Na^+ 142.0, K^+ 5.0, Mg^{2+} 1.5, Ca^{2+} 2.5, Cl^- 147.8, HCO_3^{2-} 4.2, HPO_4^{2-} 1.0 and SO_4^{2-} 0.5 mM). The samples were immersed in the electrolyte for 0.5 h prior to each electrochemical test, allowing the system to be stabilized. Polarization was carried out from -250 to 250 mV vs open circuit potential at a scan rate of 0.5 mV/s. Electrochemical impedance spectroscopy (EIS) analysis was also performed in SBF solution. The amplitude of the sinusoidal perturbing signal was 10 mV, and the frequency varied from 100 kHz to 0.01 Hz. The experimental data were fitted with Zsimwin 3.20 software.

2.5 Immersion test

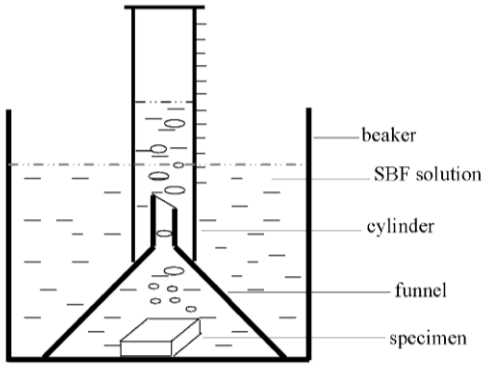

Figure 1. Schematic diagram of the device for measurement of hydrogen evolution rate

The immersion test was carried out in the sterilized bottles containing SBF solution. Each sample was immersed in a 500 mL SBF solution separately. And the temperature was kept at 37 ◦C using water bath. The hydrogen evolution method, is based on the collection of hydrogen gas during degradation of magnesium in aqueous solution. The schematic diagram of the device was shown in Fig. 1. A measuring cylinder filled with SBF solution is placed over the sample to collect the hydrogen formed during the sample's corrosion. An average of three measurements was taken for each group. The amount of hydrogen collected in the measuring cylinder over time reveals the degradation rate of the samples.

3. RESULTS AND DISCUSSION

3.1 Surface and cross-section morphologies the coatings

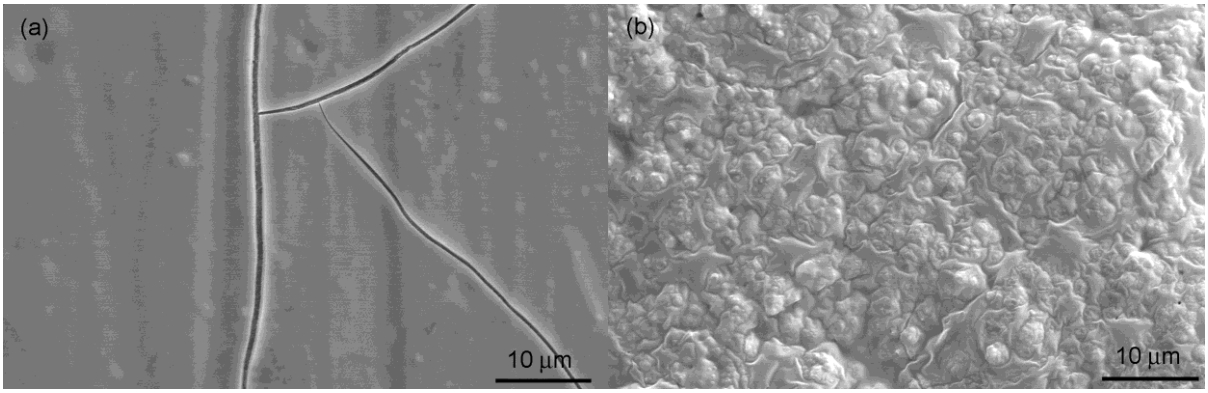

Figure 2. Surface morphologies of the sol-gel coatings: (a) T coating and (b) HT coating

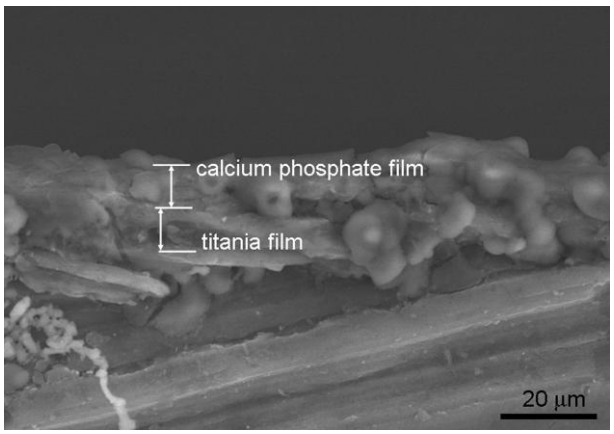

Figure 3. The cross-section morphology of HT coating

Table 1. The relative contents of elements in T and HT coatings

Element	Atomic concentration (%)	
	T coating	HT coating
O	18.64	46.80
Mg	64.29	7.27
Ti	17.08	6.39
Ca		23.64
P		15.90

Fig. 2(a) and (b) shows the surface morphology of the T coating and HT coating, respectively. Fig. 2(a) shows that micro-cracks and micro-pores are randomly distributed on the surface of titania coating. These cracks could be mainly ascribed to the sintering strain of the coating during thermal treatment. These results are very similar with the morphologies results reported by Yekehtaz et al. [24].

Such a cracked surface is beneficial to adhesive strength between the titania and calcium phosphate layers because the coated calcium phosphate gel can subsequently penetrate into the cracks and cover the surface of the titania layer completely, so that the two layers can bond closely by occlusion. Therefore, the cracked surface of the titania layer could be expected to improve the quality of the calcium phosphate layer deposition in the following process. As shown in Fig. 2(b), the micro-cracks and micro-pores disappeared and the coating is dense and compact. Some particles could be observed easily probably due to the conglomeration during the heat treatment process. This surface morphology is very similar to that reported previously on a HA/titania sol-gel coating formed on titanium substrate. It indicated that calcium phosphate sol can penetrate into the cracks and occlude with the titania layer [25, 26]. Table 1 shows the relative contents of the elements in the T coating and HT coating. Ti is detected on the surface of T coating, and Ca, P can be detected on the surface of HT coating. Fig. 3 shows the cross-section morphology of the calcium phosphate/titania coating. It can be seen clearly that the coating is integrated firmly with magnesium substrate by sintered interlocking. The calcium phosphate layer binds completely with the titania layer, and the tow layer fuses bind each other. The thickness of the titania layer and calcium phosphate layer is about 6 and 4 μm, respectively.

3.2 Phase and chemical composition of the coatings

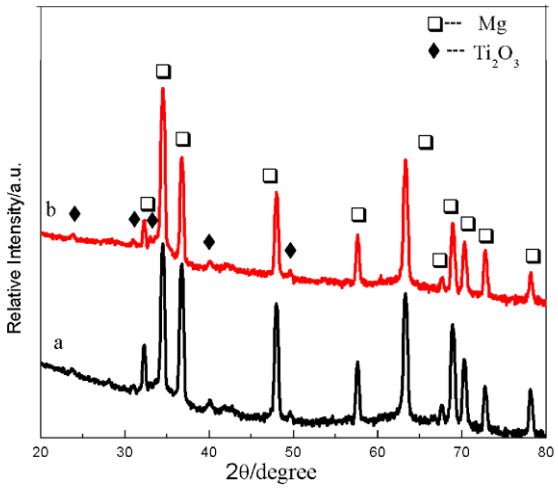

Figure 4. XRD patterns of the sol-gel coatings: (a) T coating and (b) HT coating

Fig. 4 shows the XRD patterns of the T coating and HT coating. It can be seen that the T coating is composed of Ti_2O_3. The intensity of Mg peaks corresponding to the substrate is very strong, indicating that X-ray could easily penetrate the coating. No new phases are detected in the HT coating compared to T coating. Although, there are certain amounts of Ca and P element which can be detected in the HT coating by EDS, it is noticed that no peaks of crystal phase associated with calcium and phosphate can be seen in the XRD patterns, which may be related to the amorphous state. It is reported that the sol-gel initial crystallization temperature is about 600 ^{o}C [20, 27, 28].

3.3 The adhesion strength of the coatings

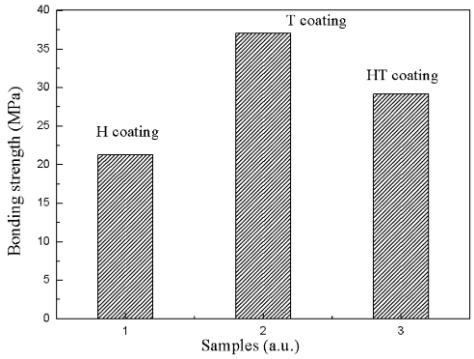

Figure 5. Bonding strength of the sol-gel coatings

A good adhesion is not only important to maintain the coating on the magnesium substrate, but also influence the corrosion behavior. The bonding strength of the T coating and HT coating on AZ31 magnesium alloy is represented in Fig. 5. The H coating with calcium phosphate deposited directly on Mg substrate without the titania layer was also tested for the purpose of comparison. The T coating processes the highest bonding strength, and the H coating exhibits the lowest bonding strength. The bonding strength of HT coating is significant superior than H coating, although the thickness of HT coating is much higher than that of H coating. It is acknowledge that the bonding strength decreases with increasing the thickness of the coating. So the results suggest that the titania buffer layer improved the bonding strength of the calcium phosphate. Based on previous researches [29], the heat treatment temperature has obvious effect on the bonding strength between the coating and the substrate, the bonding strength increase with increasing the heat treatment temperature. Kim [23] reported that the highest bonding strength was 55 MPa for the HA/TiO2 double layer on titanium substrate after heat treatment at 500 ^{o}C. Because of low melting point and poor heat resistance of magnesium alloys, it is hard to improve the bonding strength to 55 MPa only by improving the heat treatment temperature.

3.4 Electrochemical behaviors

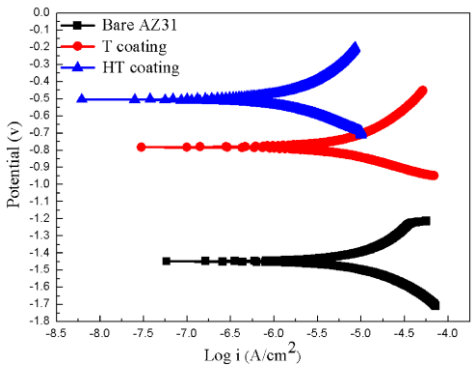

Figure 6. Polarization curves of bare magnesium and the sol-gel coatings

Table 2. The results of potentiodynamic polarization test in SBF solution

Samples	E_{corr} (V)	I_{corr} (A/cm^2)
sub	-1.45	8.25×10^{-6}
T coating	-0.78	5.26×10^{-6}
HT coating	-0.50	1.22×10^{-6}

Figure 6 shows the electrochemical polarization curves of the untreated AZ31 magnesium alloy and the different coated magnesium alloy samples in SBF solution at 37 ^{o}C. The corrosion potential (E_{corr}) and the corrosion current density (I_{corr}) extracted from the potentiodynamic polarization curves via tafel region extrapolation and the values of these parameters are summarized in Table 2. It can be seen that all the coatings have enhanced the corrosion resistance of the substrate. The corrosion potential with T coating shifted positively about 670 mV compared with the substrate, and the corrosion current density (I_{corr}) decreased from 8.25×10^{-6} A/cm^2 for the substrate to 5.26×10^{-6} A/cm^2 for T coating. For HT coating, the corrosion current density (I_{corr}) further reduced and corrosion potential (E_{corr}) enhanced as compared to T coating. This implied that compared with the substrate, the T coating improved the corrosion resistance to some extent and the HT coating could improve the corrosion resistance again.

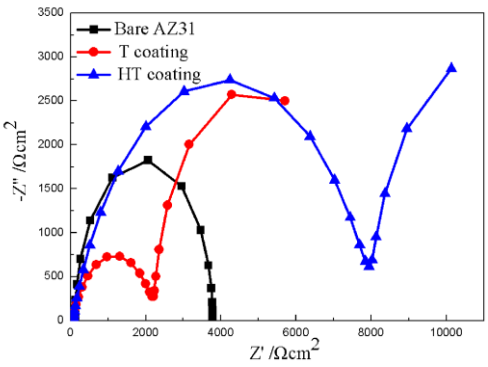

Figure 7. EIS spectra of bare magnesium alloy and the sol-gel coatings

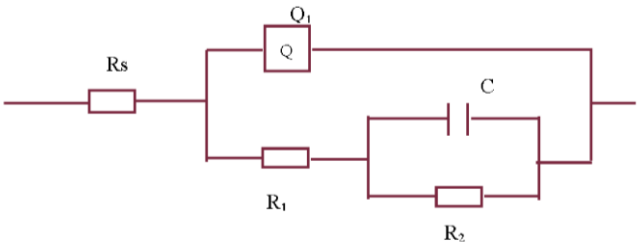

Figure 8. Simplified structure sketch of the sol-gel coatings with equivalent circuit

Table 3. Fitting results of EIS plots of the magnesium alloy AZ31 with sol-gel coatings

Samples	R_s ($\Omega.cm^2$)	$Q_{1\text{-}Y0}$ ($\Omega^{-1}.cm^{-2}.s^{-n}$)	$Q_{1\text{-}n}$	R_1 ($\Omega.cm^2$)	C ($F.cm^{-2}$)	R_2 ($\Omega.cm^2$)
Sub	1.2×10^{3}				1.8×10^{-5}	3.66×10^{3}
T coating	51.5	1.36×10^{-5}	0.80	5.23×10^{3}	2.15×10^{-3}	5.24×10^{3}
HT coating	56.3	6.06×10^{-6}	0.80	8.06×10^{3}	3.65×10^{-3}	5.91×10^{3}

Electrochemical impedance spectroscopy (EIS) was employed to investigate the corrosion characteristics of the coatings and bare substrate in SBF solution, and the resultant Nyquist plots of the T coating, HT coating and bare substrate are presented in Fig. 7. In order to better understand the corrosion behavior of these coatings, it is necessary to find an equivalent circuit to describe the impedance behavior. Taking the typical EIS plots and the morphological structure of the coatings into account, the EIS equivalent circuits for the coatings is proposed and showed in Fig. 8. The Rs represents the resistance of the electrolyte solution while R_1 and the constant phase elements (CPE Q_1) correspond to the resistance of the sol-gel film. R_2 and the capacitor C associate to the charge transfer process at the metal/electrolyte interface. Fitted parameters of the equivalent circuit for sol-gel coatings are given in Table 3. As seen from the EIS plots and Table 3, the corrosion resistance of the magnesium substrate is significantly increases with coating sol-gel layer. This indicates that the sol–gel layer provides an effective barrier against corrosive ions ingress during EIS tests. Furthermore, the corrosion resistance of HT coating increases compared to T coating. These results coincide with the results of potentiodynamic polarization. A similar study reported that the sol-gel coating could significantly increase the corrosion resistance of magnesium alloy, by forming barrier layer and preventing the corrosion ions from penetrating into the magnesium substrate [30].

3.5 Immersion testing

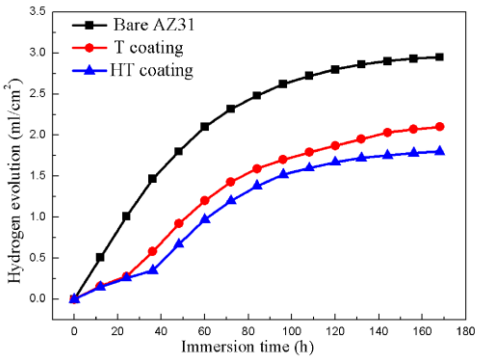

Figure 9. The hydrogen evolution volume as a function of immersion time

Fig. 9 shows the result of the hydrogen evolution tests. The substrate shows the highest evolution rate and followed by T coating, and the HT coating exhibits the slowest hydrogen evolution

rate. For the substrate, at first the hydrogen evolves volume increases rapidly, after which, the slope decreased with time. The reason for the change of the hydrogen evolves is that the substrate and SBF solution have large contact area at initial time, which could increase the corrosion reaction. Subsequently, the hydrogen evolves is slower than before, may be due to the formation of deposition coating, which blocked the corrosive intermediate contact with the substrate. And for the sol-gel coatings, at initial time the hydrogen evolves volume showed a slow increase, because that the corrosive intermediate must diffuse through the coating. Subsequently, the rate is rapider than before since the corrosive intermediate penetrated though the coating and contacted with the substrate. With further increase in immersion time, the hydrogen evolution rate shows a slowly increase again, because of the formation of corrosion products. Ghoneim et al. reported that the formation of the corrosion product layer, and the layer reduce the corrosion rate of the magnesium alloy [31].

4. CONCLUSIONS

In the present investigation, calcium phosphate/titania coating was successfully deposited on AZ31 magnesium alloy. Observations revealed that the titania coating exhibited a cracked surface. The cracks were filled in and completely covered by the subsequent calcium phosphate coating. The calcium phosphate coating displayed a compact and dense structure. The insertion of titania layer significantly improved the bonding strength of the calcium phosphate layer to the substrate. The sol-gel coatings improved the corrosion resistance and reduced the hydrogen evolves volume of magnesium alloy in SBF solution, the HT coating possessed the best corrosion resistance and the lowest hydrogen evolves volume.

ACKNOWLEDGEMENT
This work was financially supported by the Fundamental Research Funds for the Central Universities (Grant No. HIT. NSRIF. 2010066), Natural Science Foundation of Heilongjiang Province (No. E201006), key scientific and technological projects of Heilongjiang Province (No.GC10A107) of China, Natural Science Foundation of Heilongjiang Province of China under Grant (No.E200905), Scientific Research Foundation for Young Scholars, Harbin of Heilongjiang Province of China (No. 2010RFQXS114) and Doctoral Fund of Ministry of Education of China (No. 20092302120036).

References

1. L. Choudhary, R.K.S. Raman, *Acta Biomater.* 8 (2012) 916-923.
2. F. Witte, *Acta Biomater*, 6 (2010) 1680-1692.
3. M.P. Staiger, A.M. Pietak, J. Huadmai, G. Dias, *Biomaterials*, 27 (2006) 1728-1734.
4. Z.J. Wei, H. Du, E.L. Zhang, *Surf. Interface Anal,* 43 (2011) 791-794.
5. F. Witte, V. Kaese, H. Haferkamp, E. Switzer, A. Meyer-Lindenberg, C.J. Wirth, H. Windhagen, *Biomaterials*, 26 (2005) 3557-3563
6. X.N. Gu, X.L. Li, W.R. Zhou, Y. Cheng, Y.F. Zheng, *Biomed. Mater,* 5 (2010) 1-7.
7. M. Thomann, C. Krause, N. Angrisani, D. Bormann, T. Hassel, H. Windhagen, A. Meyer-Lindenberg, J. Biomed. *Mater. Res. A,* 93A (2010) 1609-1619.

8. T. Kraus, S.F. Fischerauer, A.C. Hanzi, P.J. Uggowitzer, J.F. Loffler, A.M. Weinberg, *Acta Biomater,* 8 (2012) 1230-1238.
9. H. Hornberger, S. Virtanen, A.R. Boccaccini, *Acta Biomater,* 8 (2012) 2442-2455.
10. C.L. Dai, H. Guo, J.X. Lu, J.L. Shi, J. Wei, C.S. Liu, *Biomaterials,* 32 (2011) 8506-8517.
11. J.N. Li, Y. Song, S.X. Zhang, C.L. Zhao, F. Zhang, X.N. Zhang, L. Cao, Q.M. Fan, T.T. Tang, *Biomaterials,* 31 (2010) 5782-5788.
12. D. Gopi, S. Nithiya, E. Shinyjoy, L. Kavitha, *Spectrochim. Acta. Part A,* 92 (2012) 194-200.
13. S. Tarafder, S. Bodhak, A. Bandyopadhyay, S. Bose, *J. Biomed. Mater. Res,* 97B (2011) 306-314.
14. Y.J. Zhang, G.Z. Zhang, M. Wei, *J. Biomed. Mater. Res,* 89B (2009) 408-414.
15. S. Keim, J.G. Brunner, B. Fabry, S. Virtanen, *J. Biomed. Mater. Res,* 96B (2011) 84-90.
16. M. Tomozawa, S. Hiromoto, *Acta Mater,* 59 (2011) 355-363.
17. K. Yu, L.J. Chen, J. Zhao, S.J. Li, Y.L. Dai, Q. Huang, Z.M. Yu, *Acta Biomater,* 8 (2012) 2845-2855.
18. R.G. Guan, I. Johnson, T. Cui, T. Zhao, Z.Y. Zhao, X. Li, H.N. Liu, *J. Biomed. Mater. Res,* 100A (2012) 999-1015.
19. E.C. Meng, S.K. Guan, H.X. Wang, L.G. Wang, S.J. Zhu, J.H. Hu, C.X. Ren, J.H. Gao, Y.S. Feng, *Appl. Surf. Sci,* 257 (2011) 4811-4816.
20. A. Roy, S.S. Singh, M.K. Datta, B. Lee, J. Ohodnicki, P.N. Kumta, *Mater. Sci. Eng. B,* 176 (2011) 1679-1689.
21. C.E. Wen, W. Xu, W.Y. Hu, P.D. Hodgson, *Acta Biomater,* 3 (2007) 403-410.
22. S. Chen, S.K. Guan, S.S. Hou, L.G. Wang, S.J. Zhu, J. Wang, W. Li, *Surf. Interface Anal,* 43 (2011) 1575-1580.
23. H.W. Kim, Y.H. Koh, L.H. Li, S. Lee, H.E. Kim, *Biomaterials,* 25 (2004) 2533-2538.
24. M. Yekehtaz, F. Sittner, R.U. Carrion, S. Flege, J. Brotz, W. Ensinger, Thin solid films, 518 (2010) 5223-5226.
25. P.A. Ramires, A. Romito, F. Cosentino, E. Milella, *Biomaterials,* 22 (2001) 1467-1474.
26. E. Milalla, F. Cosentino, A. Licciulli, C. Massaro, *Biomaterials,* 22 (2001) 1425-1431.
27. M.F. Hsieh, L.H. Perng, T.S. Chin, *Mater. Chem. Phys,* 74 (2002) 245-250.
28. Y. Bai, S. Park, H.H. Park, M.H. Lee, T.S. Bae, W. Duncan, A. Swain, *Surf. Interface Anal,* 43 (2011) 998-1005.
29. D.M. Liu, Q. Yang, T. Troczynski, W.J. Tseng, *Biomaterials,* 23 (2002) 1679-1687.
30. M.B. Kannan, Mater. Lett, 64 (2010) 739-742.
31. A.A. Ghoneim, A.M. Fekry, M.A. Ameer, Electrochim. Acta, 55 (2010) 6028-6035.